Journal of Inorganic Biochemistry 181 (2018) 65–73

Contents lists available at ScienceDirect

Journal of Inorganic Biochemistry

journal homepage: www.elsevier.com/locate/jinorgbio

Dynamics of dehaloperoxidase-hemoglobin A derived from NMR relaxation spectroscopy and molecular dynamics simulation

Jing Zhao[a], Mengjun Xue[b], Dorota Gudanis[c], Hanna Gracz[a], Gerhard H. Findenegg[b], Zofia Gdaniec[c], Stefan Franzen[a,*]

[a] Department of Chemistry, North Carolina State University, Raleigh, NC 27695, United States
[b] Institut für Chemie, Stranski-Laboratorium, TC 7, Technische Universität Berlin, Straße des 17, Juni 124, 10623 Berlin, Germany
[c] Institute of Bioorganic Chemistry, Polish Academy of Sciences, Z. Noskowskiego 12/14, 61-704 Poznań, Poland

ARTICLE INFO

Keywords:
Multifunctional-enzyme
Peroxidase
Peroxygenase
Protein dynamics
Model-free analysis

ABSTRACT

Dehaloperoxidase-hemoglobin is the first hemoglobin identified with biologically-relevant oxidative functions, which include peroxidase, peroxygenase and oxidase activities. Herein we report a study of the protein backbone dynamics of DHP using heteronuclear NMR relaxation methods and molecular dynamics (MD) simulations to address the role of protein dynamics in switching from one function to another. The results show that DHP's backbone helical regions and turns have average order parameters of $S^2 = 0.87 \pm 0.03$ and $S^2 = 0.76 \pm 0.08$, respectively. Furthermore, DHP is primarily a monomer in solution based on the overall tumbling correlation time τ_m is 9.49 ± 1.65 ns calculated using the prolate diffusion tensor model in the program *relax*. A number of amino acid residues have significant R_{ex} using the Lipari-Szabo model-free formalism. These include Lys^3, Ile^6, Leu^{13}, Gln^{18}, Arg^{32}, Ser^{48}, Met^{49}, Thr^{56}, Phe^{60}, Arg^{69}, Thr^{71} Cys^{73}, Ala^{77}, Asn^{81}, Gly^{95}, Arg^{109}, Phe^{115}, Leu^{127} and Met^{136}, which may experience slow conformational motions on the microseconds-milliseconds time scale according to the model. Caution should be used when the model contains > 4 fitting parameters. The program *caver3.0* was used to identify tunnels inside DHP obtained from MD simulation snapshots that are consistent with the importance of the Xe binding site, which is located at the central intersection of the tunnels. These tunnels provide diffusion pathways for small ligands such as O_2, H_2O and H_2O_2 to enter the distal pocket independently of the trajectory of substrates and inhibitors, both of which are aromatic molecules.

1. Introduction

Dehaloperoxidase-hemoglobin (DHP) is a coelomic hemoglobin first isolated from the marine annelid *Amphitrite ornata* [1]. As a member of globin superfamily, DHP shares a similar 3-over-3 α-helical bundle folded structure with many myoglobins and hemoglobins [2]. However, the DHP sequence is truncated relative to the majority of globins. DHP possesses 137 amino acids while typical mammalian globins have circa 153 amino acids. Moreover, DHP's sequence homology with other globins is < 20% [3]. DHP was first recognized as a hemoglobin in 1977 [1]. The second function of DHP was discovered in 1996 when a dehaloperoxidase activity was first reported [1, 4–6]. The third and fourth functions of DHP were revealed in 2014, when DHP was found to possess peroxygenase and oxidase activities as well [7, 8]. The substrates of DHP are brominated compounds, which are produced as repellants by a number of other organisms found in benthic ecosystems. As the most abundant protein in *A. ornata* and a heme protein, it appears that the enzymatic activities of DHP may have evolved as means of protection against the toxicity of significant concentrations of brominated compounds. *A. ornata* is immobile and therefore must withstand toxins that can build up in the benthic sediments. Therefore, our hypothesis is that DHP is a multi-functional protein with a relatively simple structure. As such, it may also serve as a model for the study of the uniqueness of structure-function relationships in hemoproteins.

The multi-functional properties of DHP are consistent with the relatively large volume of the distal pocket above the heme, which can accommodate a variety of brominated aromatic substrates mentioned above and even the amino acids phenylalanine and tyrosine [9–13]. Substrate and inhibitor binding in DHP have been studied using a variety of methods. The binding of various inhibitors and substrates has been characterized by X-ray crystallography, which showed native substrate 2,4,6-TBP and 2,4,6-TCP deeply bound in the distal pocket on

Abbreviations: DHP A, dehaloperoxidase-hemoglobin A; HSQC, heteronuclear single quantum coherence; 2,4,6-TBP, 2,4,6-tribromophenol; 2,4,6-TCP, 2,4,6-trichlorophenol; 4-BP, 4-bromophenol; MD, molecular dynamics; NMR, nuclear magnetic resonance

* Corresponding author.
E-mail address: franzen@ncsu.edu (S. Franzen).

https://doi.org/10.1016/j.jinorgbio.2018.01.006
Received 29 June 2017; Received in revised form 11 December 2017; Accepted 7 January 2018
Available online 12 January 2018
0162-0134/

the α-edge of the heme [10, 14]. Studies using ^{1}H NMR, ^{19}F NMR and ^{1}H-^{15}N HSQC spectroscopy have also provided evidence for interactions of aromatic substrates both internally and externally to the protein in solution [15, 16]. Assignments of the amide nitrogens using ^{1}H-^{15}N N HSQC show that internal substrate binding causes a significant change in the chemical shift specifically of residues in the distal pocket [15, 17]. Fourier transform infrared spectroscopy (FTIR) has also been used to characterize interactions between internalized phenolic substrates and heme-bound CO [18, 19]. These measurements are complemented by studies of photo-dissociation of the CO molecule by temperature derivative spectroscopy and flash photolysis to provide further evidence that 2,4,6-TBP, 4-BP and other molecules bind in the distal pocket and modulate the binding of diatomic ligands to the heme iron [18]. Resonance Raman spectroscopy has been used to investigate the binding affinity of substrates and inhibitors in competition with the H_2O ligand that weakly coordinates to the ferric heme [20]. This competition is pertinent since six-coordinate metaquo and five-coordinate ferric heme are in equilibrium in the ferric "resting state" of DHP at room temperature. Because the dominant function of DHP as an oxygen transport protein requires that the iron be in the ferrous form, it may be that the ferric metaquo and aquo forms are not biologically relevant. Nonetheless, it is important to study the reactivity of the ferric form of DHP since every other known peroxidase or peroxygenase has a ferric resting state. To add to the structural picture, an efficient and quantitative method to determine the relative binding affinity of different internal binding substrates was developed based on competitive fluoride ion binding to the heme iron [11]. All of these experimental results point to the fact that DHP is capable of accommodating a large number of different of aromatic molecules in the distal pocket and that there are at least two modes of internal binding in addition to the external substrate binding site on the protein surface. The external or surface binding site permits the rapid release of a substrate radical intermediate in a ping-pong peroxidase mechanism [21, 22]. The entry of substrates and inhibitors into the distal cavity required for peroxygenase and oxidase activity, involves a dynamic fluctuation in structure. So too does the binding of inhibitors of the peroxidase activity such as 4-bromophenol, which has been studied by steered molecular dynamics (SMD) simulations [23]. The dynamic fluctuations involved in the interaction of aromatic molecules are distinct from the much smaller changes in structure required for diatomic O_2 or H_2O_2 binding. The evidence to date also begs the question whether there is more than one entrance/exit route for the two types of molecules needed for DHP function, the phenolic/indolic substrates and heme-iron ligands, O_2 or H_2O_2. While the concept of binding pathways has a long history in studies of ligand binding in hemoproteins [24–28], it takes on a new importance in a globin where a number of different molecules can compete for space in the distal pocket and two different types of molecules must bind. This aspect also would benefit from studies of protein dynamics in solution.

Each of the four characterized functions of DHP, specifically the oxygen storage and transport, peroxidase, peroxygenase and oxidase functions require either O_2 or H_2O_2 to diffuse into the distal pocket to reach the heme iron atom. One method for identifying ligand transport paths is to use a tunnel calculation based on the X-ray crystal structure coordinates [2, 9, 10, 17, 29–32]. Since tunnels tend to have quite small radii the analysis must be combined with dynamic changes in structure to properly account for small molecule entry and exit. Protein dynamics are also important for entry and exit of substrates, which involves much larger conformational changes than transport of O_2 or H_2O_2. Characterization of DHP's protein dynamics will provide crucial insight into structure-function relationships and the mechanisms whereby protein-ligand interactions result in multi-functional capability [33, 34].

The present work describes a study of DHP in solution by heteronuclear relaxation NMR spectroscopy. The NMR relaxation measurements provide information on backbone dynamics on the picosecond and nanosecond time scales, which are relevant for conformational fluctuations of the protein that link substrate binding to functional switching [35–42]. The analysis presented here is based on amide proton assignments from a previous NMR study [17]. Combining these results with MD simulations and previous X-ray crystallographic structures of the two Xe binding sites of DHP [31, 32], we are able to map out the tunnel networks and correlate them with dynamic motion of the peptide backbone. This study complements previous experimental work and provides an important advance in our understanding of the multi-functional nature of DHP by showing that methionine residues are particularly active in the distal pocket region and providing further evidence for DHP protein-protein interactions in solution.

2. Material and methods

2.1. Protein expression, labeling, and purification

The pET-16b vector containing the 6XHis-tagged DHP A gene was transformed into BL21 (DE3) *E. coli* cells. The cells were plated onto LB agar plates containing 100 μg/mL ampicillin (Amp) and allowed to grow for about 18 h at 37 °C. Subsequently, *E. coli* colonies were transferred to 5 mL × 4 LB broth starter growth tubes supplemented with 100 μg/mL ampicillin. The starter growths were incubated in a shaker at 37 °C for 8 h. The cells were pelleted from the starter growths via the centrifugation at 5000 rpm for 20 min at 4 °C. The cell pellets were resuspended in 10 mL × 4 of ^{15}N isotopically-labeled M9 minimal medium (6.5 g Na_2HPO_4, 3.0 g NaH_2PO_4, 0.5 g NaCl, 1.0 g ^{15}NH4Cl, 4.0 g D(+)-glucose, 120 mg $MgSO_4$, 11 mg $CaCl_2$, 10 mg biotin, 10 mg thiamine-HCl, 100 mg ampicillin, 10 mg hemin for each 1 L) and these starter cultures were incubated at 37 °C for 8 h. Then each starter culture was used to inoculate M9 minimal media in a 1 L flask. The cells were grown at 37 °C and agitated at 230 rpm for 16 h. The cells were then induced with 0.3 mM IPTG for another 12 h while the incubation temperature was decreased to 25 °C. The purification of ^{15}N labeled his-tagged protein followed the same procedure for non-labeled his-tagged protein as described previously [43].

2.2. NMR sample preparation and heteronuclear relaxation measurement

^{15}N labeled protein samples were oxidized to ferric state and then prepared at a concentration of 0.8 mM–1.0 mM in 100 mM KP_i buffer, pH 7.0, containing 10% D_2O, 5 mM KCN to produce the metcyano form of DHP A. This produced a six-coordinated low spin (6cLS) ferric heme species with a spin quantum number (S = 1/2) that can be easily monitored using UV–Vis spectroscopy (Fig. S3A) [44]. The binding affinity of cyanide ion to the heme was determined by a spectroscopic titration method, giving the dissociation constant K_d = 159 ± 49 nM (Fig. S3B). The strong ligand field of the cyanide maintains the heme in the 6 coordinated low spin ferric state (S = ½). As a result, the paramagnetic effect is significantly suppressed compared to that in the high spin ferric state (S = 5/2) in the NMR experiment. It is also known that the distance dependence for dipole-dipole coupling follows a $1/r^6$ relation, therefore, the paramagnetic effect on backbone amide ^{15}N relaxation is negligible when the Fe-^{15}N distance is > 7.0 Å in the metacyano form of DHP. Based on analysis of the paramagnetic shifts we have observed hyperfine shifts of the heme methyl groups and of the side chains of Phe97 and His89. Those studies did not provide evidence for hyperfine shifts of any of the amide protons. Therefore, the paramagnetic effect on relaxation was ignored in our analysis.

All NMR experiments were conducted at 298K on the 500 MHz Bruker AVANCE II spectrometer and 700 MHz Bruker AVANCE III spectrometer equipped with a QCI CyroProbe. Relaxation delay for T_1 were: 0.1, 0.2, 0.3, 0.5, 0.6, 0.8, 1.0, 1.4 s for 500 MHz; 0.2, 0.3, 0.5, 0.7, 0.9, 1.1, 1.4, 1.7 s for 700 MHz. Relaxation delay for T_2 were: 17, 34, 68, 85, 102, 136, 170, 237 ms for 500 MHz; 17, 34, 51, 68, 85, 102, 136. 170 ms for 700 MHz. For both T_1 and T_2 experiment, 8 transients were measured during one FID with a recycle delay time of 3.0 s. For the {^{1}H}-^{15}N Nuclear Overhauser Effect (NOE) experiments, spectra

were recorded with and without the ^{1}H saturation in 10 s recycle time. Proton saturation was achieved with a train of 120 pulses prior to nitrogen excitation [45, 46].

All spectra were processed using Bruker software suite Topspin 3.2. The ^{1}H dimension was zero-filled to 4096 points while the indirectly detected ^{15}N dimension was zero-filled to 2048 points. Both dimensions were apodized with the shifted qsine function. The peak list of backbone amide N−H resonance of DHP A was generated based on previous assignment [17]. The processed spectra were analyzed with Bruker Protein Dynamics Center software. T_1 and T_2 were obtained by fitting the cross peak intensity over the time delay series to a single-exponential function $I(t) = I(0)\ \exp(-t/T_1)$ and $I(t) = I(0)\ \exp(-t/T_2)$. The standard error of the relaxation times was obtained from the uncertainty of the fits. The steady-state NOE values were determined from the ratio of peak intensities of the spectra with and without ^{1}H saturation.

2.3. Model-free analysis using relax

The open-source program *relax* 3.0.0 equipped with the dual optimization approach of model-free parameters and the global diffusion tensor proposed by d'Auvergne and Gooley was used to analyze the ^{15}N spin relaxation data of DHP A [47, 48]. Global diffusion and local "model-free" model selection was performed. First, the local correlation time (τ_m) was estimated for each spin with the initial diffusion tensor. Subsequent diffusion optimization was achieved by fitting data into four specific diffusion models: sphere; oblate spheroid; prolate spheroid and ellipsoid with the local model-free approach applied to each residue. Once all diffusion models converged, the best global diffusion model was used for each residue [49]. The extended model set (labeled *m*0 to *m*9) was used to describe the internal motion of amide N-H bond. The projections of the N−H bonds shown in Fig. S8 on the diffusion tensor depicted in Fig. S7 were used in *relax* to correct for the effect of anisotropy on the fit to the relaxation parameters for each residue. The models given in the Supporting information are: *m*0:{τ_m}; *m*1:{τ_m, S^2}; *m*2:{τ_m, S^2, τ_e}; *m*3:{τ_m, S^2, R_{ex}}; *m*4:{τ_m, S^2, τ_e, R_{ex}}; *m*5:{τ_m, S^2, S_f^2, τ_s}; *m*6:{τ_m, S^2, τ_f, S_f^2, τ_s}; *m*7:{τ_m, S^2, S_f^2, τ_s, R_{ex}}; *m*8:{τ_m, S^2, τ_f, S_f^2, τ_s, R_{ex}}; *m*9:{R_{ex}}, where S^2 is the squared generalized order parameter, τ_e is the effective internal correlation time in the original model-free formalism, τ_f and τ_s are the fast (picosecond) and slow (nanosecond) effective internal correlation time in the extended model-free formalism. R_{ex} is the contribution to R_2 ($1/T_2$) due to slow processes on the microsecond-millisecond time scale that can be ascribed to chemical exchange. The role of R_{ex} needs to be considered carefully in models that have > 4 fitting parameters. The following residues were identified with large values of R_{ex} in extended models *m7* (Leu^{13}, Gln^{18}, Ser^{48}, Leu^{127}, Met^{136}) and *m8* (Phe^{60}, Thr^{71}, Phe^{115}). The error propagation for all fitting parameters was calculated from Monte Carlo simulations [47, 48]. The CSA (^{15}N chemical shift anisotropy) value Δ was set to −172 ppm and the average amide N−H bond distance r_{N-H} was set to 1.02 Å.

2.4. Molecular dynamic simulations and trajectory analysis

Molecular dynamics (MD) simulations were performed using the scalable molecular dynamics program, NAMD with the CHARMM27 force field [50, 51]. The X-ray structure of the wild type ferrous-CO DHP A (PDB accession code 4DWU) was used to construct the isoelectronic metcyano form of DHP A for the MD simulations. Due to the allosteric behavior of distal histidine His^{55} that two conformations (open and closed) are in equilibrium, both N_δ (closed) and N_ε (open) histidine tautomers were simulated in parallel. NAMD simulations were carried out with periodic boundary conditions with a model solvated and placed in a unit cell of dimensions 50.5 Å × 57.2 Å × 60.7 Å contains 9254 water molecules and with Na^+ and Cl^- ions added to give an ionic strength of 0.15 M. The cutoff was set to 12 Å with a switching distance of 1.5 Å. The time step of 2 fs was used consistent with application of the SHAKE algorithm [52]. The calculations were carried out for a total of 40 ns simulation for each trajectory. Each simulation was preceded by minimization and a 5 ns equilibration phase. The global rotational and translational motions were removed for each 40 ns trajectory by using *carma*, which applies the Kabsch's algorithm to least-squares fit all frames to a reference frame [53]. 40,000 frames and unit vectors of amide N−H bond of 134 residues out of 137 (except the N terminus Gly^{1} and Pro^{29}, Pro^{75}) were extracted and calculated from each 40 ns simulations trajectory. The autocorrelation function of internal motion of amide N−H bond $C_I(t)$ (Eq. (4)) is calculated from the unit vector trajectory using an in-house Python script, of which the average of the ensemble is calculated for a 10 ps lapse increment from 0 to 20 ns. The squared generalized order parameter S^2 is evaluated using a 1 ns time window as the autocorrelation function converged.

2.5. Tunnel calculations

Caver 3.0 was used to explore the potential gas or solvent tunnels inside the met-cyano DHP A structure [54]. 50 snapshots during the 40 ns molecular dynamics simulation were applied for the tunnel calculations. Three positions, used as the starting points to probe the tunnels, were located: 1.) in the distal pocket above the heme; 2.) on the α-edge of the heme and 3.) on the proximal side beneath the heme. The clustered time-independent trajectories were used to construct the tunnel structures inside the protein structure, which were visualized in Pymol [55].

3. Results

The relaxation of all amino acid residues was studied based on data for R_1, R_2 and {^{1}H}-^{15}N NOE measurements at both 500 MHz and 700 MHz magnetic fields. Based on the criterion that all three experiments must be carried out at two magnetic fields, 118 out of 137 residues were available for analysis [17]. The relaxation data are shown in Fig. 1, plotted by residue number and annotated with the corresponding secondary structure. The average values of R_1, R_2 and {^{1}H}-^{15}N NOE are presented in Table 1, the complete dataset for each residue is given in the Table S1. We have observed {^{1}H}-^{15}N NOE values are consistently significantly lower in the EF and GH loop regions. It is noteworthy that the EF loop region contains the dimer interface of DHP that has been observed by X-ray crystallography. Residues Thr^{71}, Asp^{72} and Asn^{126} constitute the dimer interface by forming an intermolecular hydrogen bonding network [2, 9, 10, 29–31, 56]. The analysis of SAXS data suggests that DHP primarily exists as a monomer in solution and approximately 20% of the DHP molecules are in the dimeric form [57]. Therefore, non-covalent contacts between DHP monomer subunits are likely to be important for 20% of the DHP molecules in solution.

3.1. Reduced spectral density mapping and consistency testing

The relaxation rate R_1, R_2 and {^{1}H}-^{15}N NOE can be explicitly expressed in terms of five spectral density functions: $J(0)$, $J(\omega_N)$, $J(\omega_H + \omega_N)$, $J(\omega_H)$ and $J(\omega_H - \omega_N)$ for the amide N−H spin pair (Eqs. (S1)–(S3)) [58]. The spectral density function provides probability of finding motions at given angular frequency ω, which is attributed to ^{15}N relaxation. It is not possible to uniquely determine five spectral density values from the three measured relaxation data: R_1, R_2 and {^{1}H}-^{15}N NOE. Therefore, a standard approximation has been made for the high frequency terms such that $J(\omega_H) \approx J(\omega_H + \omega_N) \approx J(\omega_H - \omega_N)$ [46, 59]. In this approach all of the high frequency terms can be substituted by $J(0.87\omega_H)$, which reduces the number of unknown spectral densities from five to three. Thus, the explicit expression for the spectral density $J(0)$, $J(\omega_N)$ and $J(0.87\omega_H)$, can be uniquely using standard procedures [46, 59]. To analyze and visualize the reduced spectra density pairs J

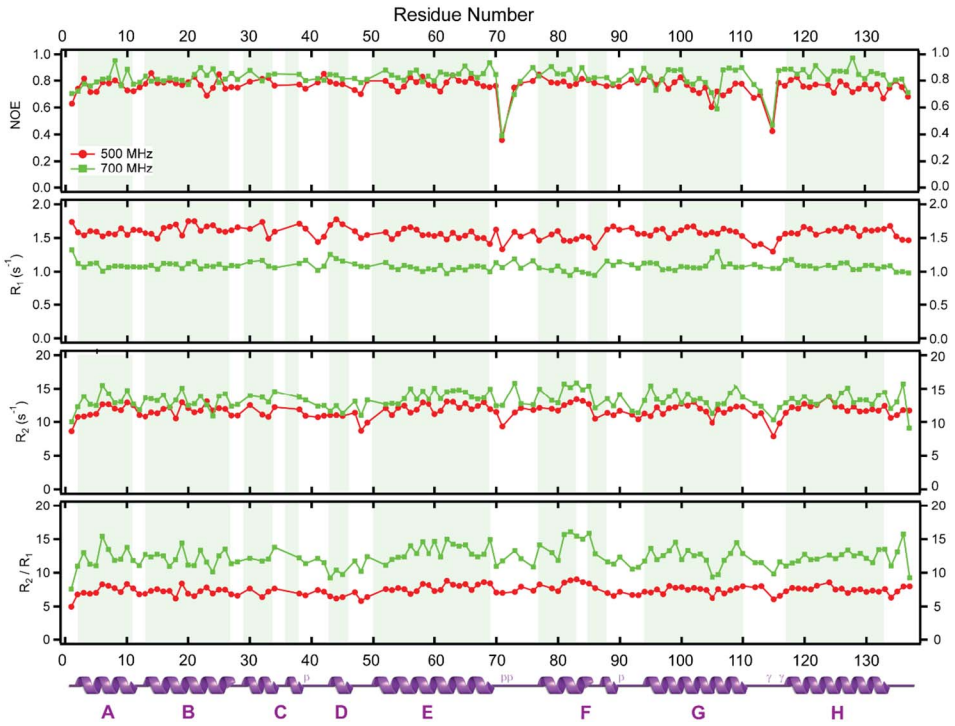

Fig. 1. NMR relaxation data {^{1}H}-^{15}N NOE, R_1, R_2 and R_2/R_1 that measured at 500 MHz (red) and 700 MHz (green). The α-helices are shown and labeled at the bottom (purple) and corresponding α-helical regions are shaded as column inside the plot. (For interpretation of the references to color in this figure legend, the reader is referred to the web version of this article.)

Table 1
Average values of R_1, R_2 and {^{1}H}-^{15}N NOE relaxation data.

	500 MHz	700 MHz
{^{1}H}-^{15}N NOE	0.760 ± 0.065	0.821 ± 0.075
R_1 (s^{-1})	1.577 ± 0.086	1.082 ± 0.062
R_2 (s^{-1})	11.67 ± 0.96	13.32 ± 1.24

Table 2
Average of J(0), J(ω_N) and J(0.87ω_H) values.

	500 MHz	700 MHz
$J(0)$ (ns/rad)	3.32 ± 0.29	3.27 ± 0.32
$J(0.87\omega_H)$ (ps/rad)	5.88 ± 1.42	3.04 ± 1.33
$J(\omega_N)$ (ns/rad)	0.31 ± 0.02	0.18 ± 0.01

(ω_N) and $J(0.87\omega_H)$, we plotted $J(\omega_N)$ and $J(0.87\omega_H)$ values as Cartesian coordinates and analyzed through Lipari-Szabo mapping (Fig. S2) [60]. The standard equations are given in the Supporting information (Eqs. (S4)–(S6)). The interested reader is referred to descriptions of the reduced spectral density mapping method [61]. The average values of $J(0)$, $J(\omega_N)$ and $J(0.87\omega_H)$ are presented in Table 2. The complete dataset is given in the Table S2.

It is a good practice to conduct consistency testing before using the two datasets for further analysis [62]. Inconsistency between datasets obtained at 500 and 700 MHz may arise from variations of pH, temperature, concentration, or the water suppression pulse sequence applied during the acquisition. The consistency of the datasets can be assessed by comparing $J(0)$, the spectral density at the zero frequency that is independent of the strength of the magnetic field. The correlation plot of two $J(0)$ for each residue calculated from reduced spectral density mapping is given in Fig. S1A. The ratios between $J(0)$ obtained at 700 MHz and 500 MHz have been plotted as the histogram in Fig. S1B. The distribution of the histogram was fitted to a Gaussian function (Blue). The center is at 0.972 with a standard deviation 0.089. Based on these comparisons we find that the datasets at 500 and 700 MHz have reasonable mutual consistency.

3.2. Model free analysis using relax

The model-free analysis of NMR relaxation data proposed by Lipari and Szabo permits this interpretation based on the idea that the correlation function of amide N−H bond vector's global motion can be factored into the two correlation functions; 1.) Overall protein tumbling and 2.) the amide N−H bond's internal motions (Eq. (1)) [63]. As a general rule, the correlation function of internal motion of amide N−H bond can be approximated by a squared generalized order parameter $S^2 \in [0, 1]$ and a single exponential decay (Eq. (2)). The limiting value $S^2 = 0$ means that the bond vector is completely flexible so that it samples all orientations isotropically. The other limit $S^2 = 1$ signifies that the bond vector is rigid and completely lacks local internal motion. The spectral density function $J(\omega)$ can be obtained by conducting a Fourier transform of the correlation function $C_I(t)$, where S^2 is the squared generalized order parameters describe the spatial restriction of the internal motion, τ_m is the overall tumbling correlation time and τ_e is the effective internal motion correlation time (Eq. (3)).

$$C_{global}(t) = C_O(t)C_I(t) \tag{1}$$

$$C_I(t) = S^2 + (1 - S^2)e^{-\frac{t}{\tau_e}} \tag{2}$$

$$J(\omega) = \frac{2}{5}\left[\frac{S^2\tau_m}{1 + (\omega\tau_m)^2} + \frac{(1 - S^2)\tau}{1 + (\omega\tau)^2}\right], \quad \frac{1}{\tau} = \frac{1}{\tau_m} + \frac{1}{\tau_e} \tag{3}$$

The principal diffusion tensors of DHP monomer structure have been calculated using the program *Hydronmr*, which gives $D_z = 1.59 \times 10^7\,s^{-1}$, $D_y = 1.84 \times 10^7\,s^{-1}$, $D_x = 1.96 \times 10^7\,s^{-1}$. Thus, $D_\perp = (D_x + D_y)/2 = 1.90 \times 10^7\,s^{-1}$ and $D_\parallel = D_z = 1.59 \times 10^7\,s^{-1}$ [64]. Therefore, the anisotropy factor is calculated as $\eta = D_\parallel / D_\perp = 1.20$ based on this analysis. These values can be compared from the analysis in the program *relax*, in which principal diffusion tensors are: $D_z = 1.44 \times 10^7\,s^{-1}$, $D_y = 1.80 \times 10^7\,s^{-1}$, $D_x = 1.99 \times 10^7\,s^{-1}$. According to these values $\eta = D_\parallel / D_\perp = 1.31$, which was used in the determination of R_1 and R_2 in the *relax*. These orientation of DHP A in this coordinate system is shown in the Supporting information (Fig. S7). Given the fact that DHP A monomer has an ellipsoid principal diffusion tensor, then $D_{iso} = (D_x + D_y + D_z)/3 = 1.79 \times 10^7\,s^{-1}$. Therefore, we

can estimate the overall tumbling correlation time, $\tau_m^{iso} = 1/(6D_{iso}) = 9.28$ ns. This estimate is in good agreement with the average τ_m of 118 residues calculated from program *relax* which gives $\tau_m = 9.49 \pm 1.65$ ns.

The two datasets obtained at 500 and 700 MHz were used to perform the model-free analysis based on the relaxation data for the 118 observed residues. The extended models set (*m*0 to *m*9) were used for model selection and fitting, the local motions of all residues were fitted to seven models (*m*1 to *m*5, *m*7 and *m*8) that can be divided as original model-free formalism (*m*1 to *m*4) and extended model-free formalism (*m*5,*m*7 and *m*8) [42, 65]. The explicit formulas of spectral density functions of eight models (*m*1 to *m*8) are given in the Supporting information.

The squared generalized order parameters S^2 provide a quantitative parameter to characterize the flexibility of the amide N−H bond vector with respect to the internal motion on the picosecond-nanosecond time scale. For 118 out of 137 residues with an order parameter S^2 available from the NMR measurements, the average of S^2 is 0.83 ± 0.10 indicates that the protein backbone is quite rigid with only limited local motions of backbone amide N−H bond. The overall rigidity is expected for DHP as a hemoglobin with a predominantly α-helical structure. The overall distribution of the order parameter S^2 clearly shows a helix-loop contrast, in which G and H helices are most rigid part in the protein structure because their average S^2 are both 0.88, whereas EF (residues 70–76) and GH (residues 111–115) loop regions are much more flexible, their average S^2 are only 0.72 and 0.69 respectively. The value of order parameter S^2 has been color mapped onto the structure as shown in Fig. 3.

The best model is selected for each residue by a statistical model-selection process to conduct the next step in the model-free analysis. The model selection results have the following distribution among the 118 residues accessible for analysis: *m*1(32), *m*2(19), *m*3(17), *m*4(12), *m*5(21), *m*7(14) and *m*8(3). 46 out of 118 residues are predicted to have non-zero term R_{ex} that attributed to the R_2 relaxation by chemical exchange. Although greater than one third of the residues of DHP have a R_{ex} term, many of them are relatively small ($R_{ex} < 1.0\ rad{\cdot}s^{-1}$) compared to what has been observed for other hemoproteins [37, 66, 67]. The residues that have $R_{ex} > 1.0\ rad{\cdot}s^{-1}$ are Lys[3], Ile[6], Leu[13], Gln[18], Arg[32], Ser[48], Met[49], Thr[56], Phe[60], Arg[69], Thr[71] Cys[73], Ala[77], Asn[81], Gly[95], Arg[109], Phe[115], Leu[127] and Met[136]. R_{ex} values extracted from the model-free formalism indicate that residues experience slow conformational motions on the microseconds-milliseconds time scale. In practice, chemical exchange between backbone amide N-H bond and bulk solvent molecules can be attributed to these slow motions. Large R_{ex} terms were observed for residues on helices B and E facing towards the distal pocket of DHP A above the heme. The other major region where significant chemical exchange could take place is in the EF loop region where the dimer interface of DHP is observed by X-ray crystallography [57]. 69 out of 118 residues experience internal motions of the amide N-H bond indicated by the non-zero effective correlation time τ_e (*m*2, *m*4, *m*5, *m*7 and *m*8). 28 out of 69 residues show internal motions on two time scales (ps and ns) that described by extended model-free formalism (*m*5, *m*7 and *m*8) for their amide N-H bond. Most of these residues are located in flexible regions such as N- and C-terminal and loops. The complete results of the model-free analysis are given in Table S3.

3.3. Molecular dynamics simulation and computed order parameter

The NMR relaxation experiment provides a direct measurement of the spectral density function $J(\omega)$. The measurement provides a connection to actual dynamics because the spectral density function is the Fourier transform of the autocorrelation function of the N−H bond vector's motion. Thus the order parameter S^2 can also be determined from the autocorrelation function of N−H bond's trajectory if the fluctuation of N−H bond is a stationary ergodic process after removing the global motion of the protein. Such stationary trajectories can be obtained by conducting MD simulations for comparison with experiment. The autocorrelation function of the amide N−H bond vector is described in Eq. (4), where P_2 is the second Legendre polynomial, $\mu(\tau)$ and $\mu(\tau + t)$ are time-dependent unit vectors that describe the spatial orientation of N-H bond in a fixed reference frame. The S^2 is the limit of autocorrelation function when time approaches to infinity (Eq. (5)). In practice, S^2 can be determined when the autocorrelation function converges.

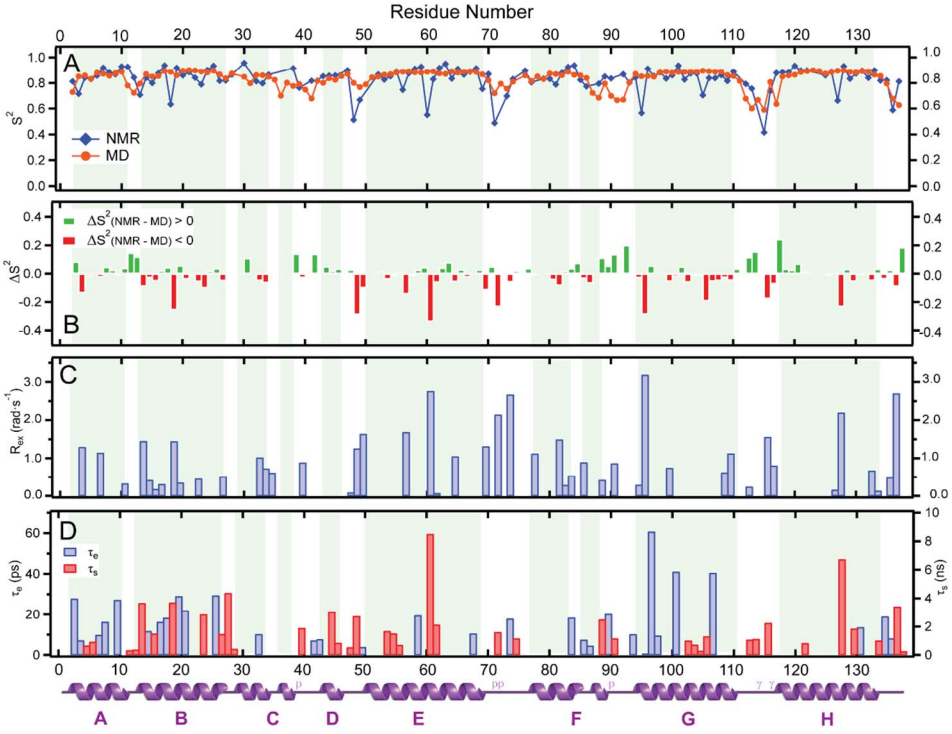

Fig. 2. (A) Comparison of generalized order parameter S^2 obtained from NMR (blue) and MD (orange) for each residue in DHPA; (B) the difference histogram of generalized order parameters S^2 between NMR and MD; (C) histogram of relaxation attribute to chemical exchange R_{ex}; (D) histogram of effective correlation time of internal motion τ_e (ps) (blue, left axis) and slow effective correlation time τ_s (ns) (red, right axis) in two different time-scales. (For interpretation of the references to color in this figure legend, the reader is referred to the web version of this article.)

$$C_I(t) = \langle P_2[\mu(\tau)\bullet\mu(\tau + t)]\rangle \quad (4)$$

$$S^2 = \lim_{t\to\infty} C_I(t) \quad (5)$$

Here, we have calculated S^2 from MD simulations and compared the simulated values with those obtained from NMR relaxation experiments. Because distal histidine His^{55} may adopt closed or open conformations, both N_δ and N_ε histidine tautomers were modeled in sets of five 40 ns simulations, the order parameters were calculated as the average of all five of these simulations (Fig. S4). The average order parameter S^2 of 134 residues from MD simulations is 0.84 ± 0.07. The order parameters calculated from MD simulations distribute in a narrower range indicated by the smaller standard deviation as compared to those from NMR. Nonetheless, the order parameters obtained from MD also presented a distinctive helix-loop contrast (Fig. S6). The average of S^2 in helix region is 0.87 ± 0.03, whereas in loop region, it is 0.76 ± 0.08. The complete dataset of S^2 calculated from MD simulation can be found at Table S4.

In general, the order parameters S^2 calculated from MD simulations are consistent with those obtained from NMR relaxation experiments (Fig. 2A, B). One major discrepancy in S^2 between NMR and MD can be observed for residues in the relatively flexible loop regions (Fig. 2B, C). The order parameters, S^2, predicted by MD simulations are generally lower than those measured by the NMR relaxation experiment except for a few residues that have significantly smaller S^2 values and larger R_{ex} terms. One issue is that local motions of flexible residues on the same timescale as the global tumbling time ($\tau_m \sim 10$ ns) cannot be distinguished from tumbling itself. As the result, these local motions are not reflected by order parameters S^2 measured in the NMR experiment. And the rigidity of those residues are overestimated in the NMR experiment. Despite this weakness, it is a reasonable assumption that the discrepancy between NMR and MD can explain the difference between the simulated and experimental order parameters, S^2.

3.4. Tunnels in the protein interior

We have used the program *Caver* 3.0 to identify tunnels that connect the internal cavities of protein to the solvent. Four major tunnels were identified that connect the distal cavity to the protein surface. They are the AB tunnel, starting from distal pocket and ending between helix A and B; the CD tunnel, connecting distal pocket to the CD loop region; the EF tunnel, starting from α-edge of the heme plane and exiting between helix E and F; and the GH tunnel, starting from a cavity above the α-edge of the heme and passing between helices G and H. These tunnels interconnect at a central location near the back of the distal cavity where a cavity inside DHP is known to exist. The two Xe binding sites that are characterized by X-ray crystallography are located within the calculated tunnels structures as shown in Fig. 3 [32] shows that the Xe1 binding site is located at starting point of tunnel CD that is the distal pocket right above the α-edge of the heme and the Xe2 binding site is on the passageway of EF tunnel that leads to protein surface.

4. Discussion

4.1. Evidence for transient dimerization in solution

DHP is a multi-functional hemoglobin that possesses the highly conserved 3-over-3 helical bundle fold, which is observed in single hemoglobin subunits and myoglobins (sperm whale, horse, human etc.) [31, 68]. Since DHP A is a crystallographic dimer in every X-ray crystal structure obtained, it is possible that DHP A also forms dimers in solution [57]. The relatively small dimer interface in the crystallized form of DHP may explain why a permanent dimer is not observed in solution. The crystallographic dimer "interface" is really just a group of three amino acids whose mutual interaction is too weak for DHP to result in a true dimer. Yet, one sees evidence of interactions in solution in SAXS and NMR data.

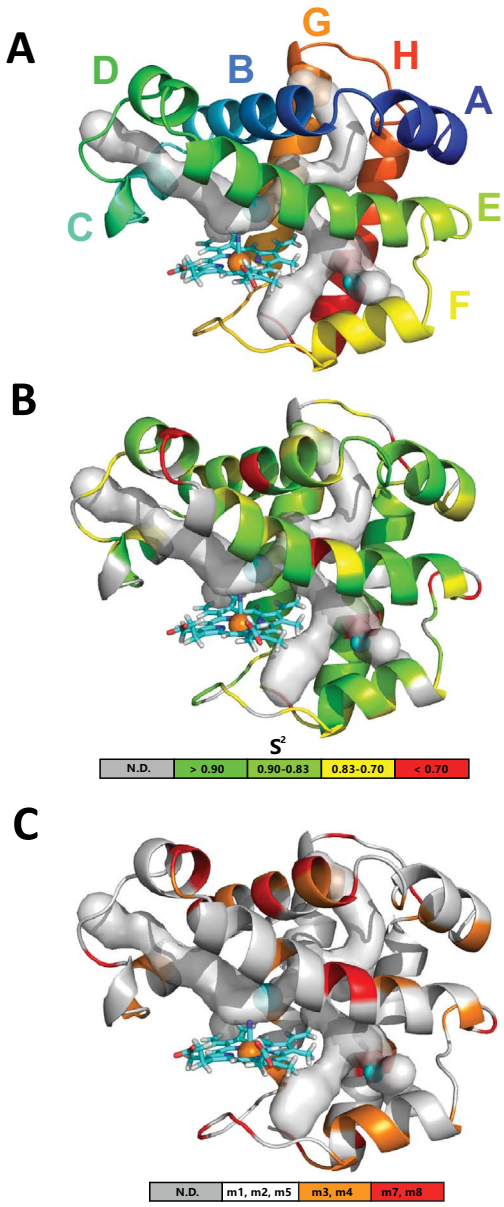

Fig. 3. Color mapping of secondary structural information and NMR model-free analysis results on the met-cyano DHP A structure. (A) Color mapped eight α-helices of DHPA with calculated tunnel structures and the two xenon binding sites. (B) Color mapped generalized order parameter S^2 on DHP A structure. (C) Color mapped model selection results of model-free analysis on the DHP A structure.

The SAXS studies provide evidence that DHP A is > 80% monomer in solution [57]. The NMR relaxation study corroborates this conclusion since the correlation time consistent with the data is that of a monomeric globin. We can compare the overall tumbling correlation time τ_m between 3-over-3 fold as well as 2-over-2 hemoglobins (Table 3). We can see that the overall tumbling correlation time τ_m is approximately proportional to the number of subunits in a hemoglobin oligomer. Because τ_m is approximately the inverse of the diffusion tensor and proportional to the size of the molecule for a spherical model (i.e. ignoring anisotropy to make a global comparison). Therefore, it is evident that DHP is indeed primarily a monomer in solution as measured by NMR relaxation experiments as well. However, NMR also informs us that there are weak interactions in solution that result in a population of transient dimers or weakly associated proteins [17].

The same dimer interface has been observed in every X-ray crystal

Table 3
Comparison between different hemoglobins.

Name	Oligomer	Fold	Ligation	τ_m (ns)	$< S^2 >$	T (°C)
Dehaloperoxidase - hemoglobin (DHP)	Monomer (> 80%)	3-on-3	Ferric-CN	9.49	0.83	25
Glycera dibranchiata hemoglobin [66]	Monomer	3-on-3	Ferrous-CO	10.3	0.93	20
Scapharca hemoglobin I [76]	Dimer	3-on-3	Ferrous-CO	17.7	0.91	25
Human hemoglobin A [81]	Tetramer	3-on-3	Ferrous-CO	31.5–33	N.A.	29
Truncated hemoglobin N [67]	Monomer	2-on-2	Ferric-CN	10	0.84	26.4
Hemoglobin of truncated lineage (GlbN) [82]	Monomer	2-on-2	Ferrous-CO	8.4	N.A.	25

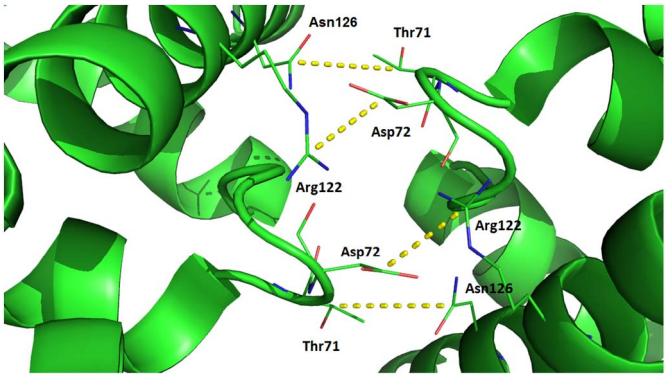

Fig. 4. Dimer interface of DHP observed in X-ray crystallography.

structure or either DHP A and B. The interface has a surface area of ~200 Å^2 and is located at EF loop region. The interprotein contacts involve residues Thr^{71}, Asp^{72} and Cys^{73} and two residues Arg^{122} and Asn^{126} on the H helix (Fig. 4) [31]. The small dimer interface area of DHP is in contrast with the extensive interface region observed in the dimeric hemoglobin from *Scapharca* and many other hemoglobins [69, 70].

The significantly lower {^{1}H}-^{15}N NOE values in the EF loop region indicates enhanced flexibility on the ps-ns time scale. Residues Thr^{71}, Cys^{73} on the EF loop and Leu^{127} on the H helix also show significantly lower order parameters S^2, consistent with the existence of rapid slower conformational change and two-time scale internal motions in the backbone amide N–H bonds. It may also be of importance that Thr^{71} and Cys^{73} are on the list of amino acids that have large rates of chemical exchange, R_{ex}. As a cautionary note, Thr^{71} is one of three amino acids that had a best fit by model *m8* requiring 6 fit parameters. At first it may appear inconsistent that an anomalously low value of S^2 is observed for residue Leu^{127}, which is in the middle of the relatively rigid H helix. However, one possible explanation for this anomaly may be that this residue is adjacent to residue Asn^{126} that is observed to be one of the critical residues corresponding to the formation of the dimer in the X-ray crystal structure. The increased dynamic activity observed in these amino acids is indicative of the change that would occur if those amino acids are alternatingly involved in formation of a dimer and return to monomer conformation. These dynamics may explain puzzling observations that have appeared in many DHP experiments as the result of transient dimer formation. Of course, a transient structure formed in < 20% of the sample would be completely elusive if were not for the fact that the very structure of the dimer is present in every single X-ray crystal structure of DHP [30, 31, 71].

One possible role for this tendency to form dimers (or even multimers) may be the formation of giant hemoglobin (erythrocruorin), which is found in the tentacles of the annelid [1]. The erythrocruorin is composed of three different proteins in a multimer with a molar mass of > 3 Md [72, 73]. The subunits that make up the “giant hemoglobin” are the two different forms of DHP, the isoforms from genes *dhpa* and *dhpb* in *A. ornata* [74] and a third as yet unknown non-heme-containing polypeptide chain [75]. However, DHP A and B alone do not form any permanent structures larger than dimers based on all of the experimental observations, discounting the formation of precipitates, which apparently lack a regular structure. Although DHP has a strong tendency to aggregate at protein concentrations of > 1.0 mM other hemoglobins and myoglobins are typically stable at such concentrations. The propensity of DHP to aggregate may be related to the transient dimerization proposed to explain the SAXS, X-ray crystallographic and NMR observations.

4.2. The role of tunnels in the regulation of substrate and heme ligand binding

Both NMR data and MD simulations indicate that DHP A has rather high backbone rigidity consistent with the high order parameters S^2 for backbone amino acids [66, 67, 76]. Table 3 shows that this is expected for DHP A as a member of the hemoglobin family. For example, the average order parameter S^2 (0.83 ± 0.10 from NMR, 0.84 ± 0.07 from MD, 25 °C) of DHP A is comparable to that of other hemoglobins (Table 3). Despite significant helix-loop contrast, the high rigidity of major B, E, G and H helices on the picosecond-nanosecond time scale are necessary to support the tunnel structures inside the protein. These dynamical tunnels likely exist in DHP A to allow it to carry out multiple functions. These channels reveal the pathways by which O_2 and H_2O_2 can diffuse into the active site and bind to the heme Fe. The possibility for multiple entry channels may derive from the differences in the various functions. It is reasonable to hypothesize that small molecule heme Fe ligands, e.g. O_2, H_2O_2 and H_2O, must diffuse into the distal pocket independently of aromatic substrates, such as halogenated phenols and indole derivatives. The tunnels observed using *caver3.0* permit rapid entry and exit of the three main small molecules O_2, H_2O_2 and H_2O though channels that do not compete with the main entry/exit channel for the substrate, which is used by the larger substrate molecules [23]. Perhaps more important than the rate of entry/exit is the fact that these tunnels suggest possible regulatory mechanisms for function.

The SMD simulations provide evidence that the distal histidine His^{55} gate in DHP can play a role similar to SWMb, but that the pocket is more flexible so much larger molecules can enter and exit [23]. Molecules as large as 4-BP do not enter the distal pocket of SWMb or any other known myoglobin or hemoglobin [56, 77, 78]. Based on the X-ray crystal structural data it is evident that substrates such as 2,4,6-TBP, 2,4,6-TCP and several indoles can also bind in the distal pocket of DHP. It seems highly likely that the substrate entrance channel in these cases is similar to the 4-BP channel identified by SMD. Combining the DHP and SWMb observations it is also evident that substrates and small molecules (O_2 and H_2O_2) may collide if they both use the same entry channel. For this reason, it is important to keep in mind that there may be alternative entry channels for the O_2 and H_2O_2 that permit regulation of the binding and of reactivity. To be sure the notion that diatomic ligands have multiple entry channels has also been advanced in studies of myoglobin. But, DHP presents a unique set of challenges that include triggering changes in function and regulating the activity once a particular cycle has been initiated.

The distal cavity functions as an internal substrate binding site for the peroxygenase and oxidase functions and as an inhibition site for

the peroxidase function [7, 17]. The modes of binding of various molecules include an α-site along the α-edge of the heme, which is most deeply buried in the globin and a β-site, in which the phenol (or indole) is perpendicular to the heme shifted off-center towards the β-edge of the heme. Regardless of the mode of binding the halogen atom in the substrates and inhibitors are always located in (or very close to) the Xe binding site in DHP. Furthermore, there is a transient docking site for unbound diatomic gas molecules in the Xe binding site as well [32]. The tunnels observed in the DHP structure intersect at the Xe binding site providing the possibility of alternative routes of entry and exit for the ligands, O_2 and H_2O_2. The evidence for a connection between these tunnels and DHP function is circumstantial, but there are numerous observations that can be explained by controlled entry and exit of ligands independent of the binding of phenolic substrates. The order of binding events (e.g. trichlorophenol and H_2O_2) has an effect on peroxidase oxidation kinetics as has been shown in experiments using double-mixing stopped flow and studies of activation of the oxy species [79]. There is evidence for a trigger event due to substrate binding that is capable of initiating the peroxidase cycle beginning from the oxy form of DHP. If H_2O_2 is added to oxy-ferrous DHP, the reaction to form compound II is extremely slow [7]. However, if a substrate such as 2,4,6-TCP is present this rate is significantly more rapid. Indeed, an intermediate species has been identified as the Fe(II)-H_2O_2 adduct using stopped-flow spectroscopy. This means that the replacement reaction of O_2 by H_2O_2 occurs at a measurable rate only when the structure is modulated by the binding of 2,4,6-TCP, which assumed to bind externally in this functional state of DHP. This behavior may arise from controlled entry of H_2O_2, but also may involve the conformation of the distal histidine, which may favor binding of H_2O_2 over O_2 in the substrate-bound conformation. In summary, tunnels may form transiently to allow H_2O_2 or O_2 to diffuse into or out of the distal pocket of DHP A in response to the binding of the larger substrate molecules, which act to trigger specific functions of the protein.

4.3. The role of chemical exchange in the protein dynamics of DHP

According to the fits in the model-free method, a significant number of residues in the structure exhibit some degree of chemical exchange. Chemical exchange as a parameter in the fitting arises when there is a slow component to the R_1 and R_2 decays. It can also be validated by MD simulations since these will also provide an independent estimate for the order parameter of the N-H bond vector. The Lipari-Szabo procedure indicates significant chemical exchange (R_{ex}) for amino acids Lys^3, Ile^6, Leu^{13}, Gln^{18}, Arg^{32}, Ser^{48}, Met^{49}, Thr^{56}, Phe^{60}, Arg^{69}, Thr^{71} Cys^{73}, Ala^{77}, Asn^{81}, Gly^{95}, Arg^{109}, Phe^{115}, Leu^{127} and Met^{136}. A number of these residues (Lys^3, Ile^6, Arg^{32}, Thr^{56}, Thr^{71}, Cys^{73}, Gly^{95}, Leu^{127}) are on the surface of the protein and it is not surprising that they would have significant contribution from chemical exchange. Three of these amino acids are in or adjacent to the dimer interface region as well as being on the surface (Thr^{71}, Cys^{73} and Leu^{127}). The importance of the mobility of Thr^{56} has been studied by systematic mutations at position 56 to understand how the dynamics of this amino acid affect the neighboring distal histidine, His^{55} [80]. Finally, we note that that 5 out of 7 sulfur containing residues (Met^{49}, Met^{69}, Met^{108}, Met^{136} and Cys^{73}) in DHP A show chemical exchange on their backbone amides. Three of these are significant and the other two have neighboring amino acids with significant chemical exchange (defined as $R_{ex} > 1.0\,\mathrm{rad\,s^{-1}}$). DHP A is rich in methionines compared to other hemoglobins. The tendency of DHP A to maintain a ferrous oxidation state may depend on redox active amino acids, including these methionines. Given the uncertainties in the interpretation of R_{ex} it is not possible to say whether there is any functional significance to the observed fits. But, it is worth noting because future studies will focus on the role of these methionines in the redox regulation of DHP.

5. Conclusion

In conclusion, we have quantitatively described four dynamic features of DHP A from *Amphitrite ornata* by using heteronuclear NMR relaxation methods combined with MD simulations. These features are 1.) α-helices are uniformly rigid, 2.) turn and loop regions are consistently less rigid and more variable, 3.) the residues Thr^{71}, Cys^{73} and Leu^{127} in the crystallographic dimer have low order parameters, and 4.) many of the amino acids that show significant exchange are on the surface. While many of these observations are expected, this study provides an important baseline study of dynamic amino motions in DHP A that will be essential to understand the differences between DHP A and B and the potential dynamic effects of internal substrate binding in both forms of DHP. The functional question for DHP is how the globin regulates both small molecule and aromatic substrate binding in the same pocket. Thus, we have also studied the narrow tunnels that permit the exit and entry of small molecules, O_2, H_2O_2 and H_2O. These entry and exit channels may complement the pathway for substrate (and inhibitor) entry into the distal pocket by another route. We hypothesize that tunnels are essential passageways required for DHP to carry out its multiple functions, including oxygen transport, peroxidase, peroxygenase and oxidase activity. The switching between these functions involves subtle aspects of the whole protein structure triggered by substrate binding [18]. While X-ray crystallography has provided an essential foundation for understanding dimerization and internal substrate binding geometries, NMR evidence has provided the most comprehensive view yet of the systematic nature of conformational changes in the DHP A that may complement His^{55} in providing mechanisms of function switching and regulatory control.

Acknowledgement

This work was supported by Army Research Office grant 57861-LS and NSF grant CHE-1507947. The collaboration with researchers in Poznan, Poland was supported by a fellowship received by S.F. from the Fulbright Foundation. GF and MX acknowledge support by the German Research Foundation (DFG) in the framework of IRTG 1524.

Appendix A. Supplementary data

Supplementary data to this article can be found online at https://doi.org/10.1016/j.jinorgbio.2018.01.006.

References

[1] R.E. Weber, C. Mangum, H. Steinman, C. Bonaventura, B. Sullivan, J. Bonaventura, Comp. Biochem. Physiol. A Physiol. 56 (1977) 179–187.
[2] M.W. LaCount, E. Zhang, Y.P. Chen, K. Han, M.M. Whitton, D.E. Lincoln, S.A. Woodin, L. Lebioda, J. Biol. Chem. 275 (2000) 18712–18716.
[3] X. Bailly, C. Chabasse, S. Hourdez, S. Dewilde, S. Martial, L. Moens, F. Zal, FEBS J. 274 (2007) 2641–2652 (Blackwell Publishing Ltd).
[4] Y.P. Chen, S.A. Woodin, D.E. Lincoln, C.R. Lovell, J. Biol. Chem. 271 (1996) 4609–4612.
[5] S. Sun, M. Sono, J. Du, J.H. Dawson, Biochemistry 53 (2014) 4956–4969 (American Chemical Society).
[6] S. Franzen, J. Belyea, L.B. Gilvey, M.F. Davis, C.E. Chaudhary, T.L. Sit, S.A. Lommel, Biochemistry 45 (2006) 9085–9094 (American Chemical Society).
[7] D.A. Barrios, J. D'Antonio, N.L. McCombs, J. Zhao, S. Franzen, A.C. Schmidt, L.A. Sombers, R.A. Ghiladi, J. Am. Chem. Soc. 136 (2014) 7914–7925 (American Chemical Society).
[8] N.L. McCombs, J. D'Antonio, D.A. Barrios, L.M. Carey, R.A. Ghiladi, Biochemistry 55 (2016) 2465–2478 (American Chemical Society).
[9] L. Lebioda, M.W. LaCount, E. Zhang, Y.P. Chen, K. Han, M.M. WHitton, D.E. Lincoln, S.A. Woodin, Nature 401 (1999) 445.
[10] J. Zhao, V. de Serrano, J.J. Zhao, P. Le, S. Franzen, Biochemistry 52 (2013) 2427–2439.
[11] J. Zhao, J. Moretto, P. Le, S. Franzen, J. Phys. Chem. B 119 (2015) 2827–2838 (American Chemical Society).
[12] J. Zhao, J. Zhao, S. Franzen, J. Phys. Chem. B 117 (2013) 14615–14624.
[13] J. Du, M. Sono, J.H. Dawson, Biochemistry 49 (2010) 6064–6069 (American Chemical Society).
[14] C. Wang, L.L. Lovelace, S. Sun, J.H. Dawson, L. Lebioda, Biochemistry 52 (2013)

6203–6210 (American Chemical Society).
[15] M.F. Davis, H. Gracz, F.A.P. Vendeix, V. de Serrano, A. Somasundaram, S.M. Decatur, S. Franzen, Biochemistry 48 (2009) 2164–2172 (American Chemical Society).
[16] M.F. Davis, B.G. Bobay, S. Franzen, Biochemistry 49 (2010) 1199–1206.
[17] M.K. Thompson, M.F. Davis, V. de Serrano, F.P. Nicoletti, B.D. Howes, G. Smulevich, S. Franzen, Biophys. J. 99 (2010) 1586–1595.
[18] K. Nienhaus, P. Deng, J. Belyea, S. Franzen, G.U. Nienhaus, J. Phys. Chem. B 110 (2006) 13264–13276 (American Chemical Society).
[19] K. Nienhaus, E. Nickel, M.F. Davis, S. Franzen, G.U. Nienhaus, Biochemistry 47 (2008) 12985–12994 (American Chemical Society).
[20] F.P. Nicoletti, M.K. Thompson, B.D. Howes, S. Franzen, G. Smulevich, Biochemistry 49 (2010) 1903–1912 (American Chemical Society).
[21] H. Ma, M.K. Thompson, J. Gaff, S. Franzen, J. Phys. Chem. B 114 (2010) 13823–13829 (American Chemical Society).
[22] J. Zhao, C. Lu, S. Franzen, J. Phys. Chem. B 119 (2015) 12828–12837 (American Chemical Society).
[23] Z. Zhang, A.P. Santos, Q. Zhou, L. Liang, Q. Wang, T. Wu, S. Franzen, Biophys. Chem. 211 (2016) 28–38.
[24] F. Schotte, M. Lim, T.A. Jackson, A.V. Smirnov, J. Soman, J.S. Olson, G.N. Phillips, M. Wulff, P.A. Anfinrud, Science 300 (2003) 1944–1947.
[25] E.E. Scott, Q.H. Gibson, J.S. Olson, J. Biol. Chem. 276 (2001) 5177–5188.
[26] J. Cohen, K. Schulten, Biophys. J. 93 (2007) 3591–3600.
[27] M. Gabba, S. Abbruzzetti, F. Spyrakis, F. Forti, S. Bruno, A. Mozzarelli, F.J. Luque, C. Viappiani, P. Cozzini, M. Nardini, F. Germani, M. Bolognesi, L. Moens, S. Dewilde, PLoS One 8 (2013) e49770 (Public Library of Science).
[28] R. Fu, R. Gupta, J. Geng, K. Dornevil, S. Wang, Y. Zhang, M.P. Hendrich, A. Liu, J. Biol. Chem. 286 (2011) 26541–26554.
[29] V.S. de Serrano, M.F. Davis, J.F. Gaff, Q. Zhang, Z. Chen, E.L. D'Antonio, E.F. Bowden, R. Rose, S. Franzen, Acta Crystallogr. D Biol. Crystallogr. 66 (2010) 770–782.
[30] Z. Chen, V. De Serrano, L. Betts, S. Franzen, Acta Crystallogr. D Biol. Crystallogr. 65 (2009) 34–40.
[31] V. de Serrano, Z.X. Chen, M.F. Davis, S. Franzen, Acta Crystallogr. D Biol. Crystallogr. 63 (2007) 1094–1101.
[32] V. De Serrano, S. Franzen, Pept. Sci. 98 (2012) 27–35.
[33] A.G. Palmer, Chem. Rev. 104 (2004) 3623–3640 (American Chemical Society).
[34] V.A. Jarymowycz, M.J. Stone, Chem. Rev. 106 (2006) 1624–1671 (American Chemical Society).
[35] D. Muthu, R.E. Berry, H. Zhang, F.A. Walker, Biochemistry 52 (2013) 7910–7925 (American Chemical Society).
[36] E. Harada, M. Sugishima, J. Harada, K. Fukuyama, K. Sugase, Biochemistry 54 (2015) 340–348 (American Chemical Society).
[37] A.I. Karsisiotis, O.M. Deacon, M.T. Wilson, C. Macdonald, T.M.A. Blumenschein, G.R. Moore, J.A.R. Worrall, Sci. Rep. 6 (2016) 30447 (The Author(s)).
[38] K. Tozawa, S.J. Ferguson, C. Redfield, L.J. Smith, J. Biomol. NMR 62 (2015) 221–231.
[39] M. Fang, S. Baldelli, J. Phys. Chem. C 121 (2017) 1591–1601.
[40] A.G. Palmer, J. Williams, A. McDermott, J. Phys. Chem. 100 (1996) 13293–13310 (American Chemical Society).
[41] L.E. Kay, Nat. Struct. Biol. 5 (1998) 513–517.
[42] G.M. Clore, A. Szabo, A. Bax, L.E. Kay, P.C. Driscoll, A.M. Gronenborn, J. Am. Chem. Soc. 112 (1990) 4989–4991 (American Chemical Society).
[43] H. Ma, M.K. Thompson, J. Gaff, S. Franzen, J. Phys. Chem. B 114 (2010) 13823–13829 (American Chemical Society).
[44] G.B. Crull, H.M. Goff, J. Inorg. Biochem. 50 (1993) 181–192.
[45] L. Kay, P. Keifer, T. Saarinen, J. Am. Chem. Soc. 114 (1992) 10663–10665 (American Chemical Society).
[46] N.A. Farrow, R. Muhandiram, A.U. Singer, S.M. Pascal, C.M. Kay, G. Gish, S.E. Shoelson, T. Pawson, J.D. Forman-Kay, L.E. Kay, Biochemistry 33 (1994) 5984–6003 (American Chemical Society).
[47] E. d'Auvergne, P. Gooley, J. Biomol. NMR 40 (2008) 107–119 (Springer Netherlands).
[48] E. d'Auvergne, P. Gooley, J. Biomol. NMR 40 (2008) 121–133 (Springer Netherlands).
[49] E. d'Auvergne, P. Gooley, J. Biomol. NMR 25 (2003) 25–39 (Kluwer Academic Publishers).
[50] M.T. Nelson, W. Humphrey, A. Gursoy, A. Dalke, L.V. Kalé, R.D. Skeel, K. Schulten, Int. J. High Perform. Comput. 10 (1996) 251–268.
[51] J.C. Phillips, R. Braun, W. Wang, J. Gumbart, E. Tajkhorshid, E. Villa, C. Chipot, R.D. Skeel, L. Kalé, K. Schulten, J. Comput. Chem. 26 (2005) 1781–1802 (Wiley Subscription Services, Inc., A Wiley Company).
[52] J.-P. Ryckaert, G. Ciccotti, H.J.C. Berendsen, J. Chem. Phys. 23 (1977) 327–341.
[53] N.M. Glykos, J. Comput. Chem. 27 (2006) 1765–1768 (Wiley Subscription Services, Inc., A Wiley Company).
[54] E. Chovancova, A. Pavelka, P. Benes, O. Strnad, J. Brezovsky, B. Kozlikova, A. Gora, V. Sustr, M. Klvana, P. Medek, L. Biedermannova, J. Sochor, J. Damborsky, PLoS Comput. Biol. 8 (2012) e1002708 (Public Library of Science).
[55] Schrodinger, LLC, 2015.
[56] J. Zhao, V. de Serrano, S. Franzen, Biochemistry 53 (2014) 2474–2482 (American Chemical Society).
[57] M.K. Thompson, S. Franzen, M.F. Davis, R.C. Oliver, J.K. Krueger, J. Phys. Chem. B 115 (2011) 4266–4272 (American Chemical Society).
[58] J.W. Peng, G. Wagner, J. Magn. Reson. 98 (1992) 308–332.
[59] J.F. Lefèvre, K.T. Dayie, J.W. Peng, G. Wagner, Biochemistry 35 (1996) 2674–2686 (American Chemical Society).
[60] M. Andrec, G.T. Montelione, R.M. Levy, J. Biomol. NMR 18 (2000) 83–100.
[61] J.W. Peng, G. Wagner, J. Magn. Reson. (1969) 98 (1992) 308–332.
[62] S. Morin, S.M. Gagné, J. Biomol. NMR 45 (2009) 361–372 (Springer Netherlands).
[63] G. Lipari, A. Szabo, J. Am. Chem. Soc. 104 (1982) 4546–4559 (American Chemical Society).
[64] J. García de la Torre, M.L. Huertas, B. Carrasco, J. Magn. Reson. 147 (2000) 138–146.
[65] J. Chen, C.L. Brooks, P.E. Wright, J. Biomol. NMR 29 (2004) 243–257.
[66] B.F. Volkman, S.L. Alam, J.D. Satterlee, J.L. Markley, Biochemistry 37 (1998) 10906–10919 (American Chemical Society).
[67] P.-Y. Savard, R. Daigle, S. Morin, A. Sebilo, F. Meindre, P. Lagüe, M. Guertin, S.M. Gagné, Biochemistry 50 (2011) 11121–11130 (American Chemical Society).
[68] J.C. Kendrew, R.E. Dickerson, B.E. Strandberg, R.G. Hart, D.R. Davies, D.C. Phillips, V.C. Shore, Nature 185 (1960) 422–427.
[69] W.E. Royer, R.A. Fox, F.R. Smith, D. Zhu, E.H. Braswell, J. Biol. Chem. 272 (1997) 5689–5694.
[70] W.E. Royer Jr., J.E. Knapp, K. Strand, H.A. Heaslet, Trends Biochem. Sci. 26 (2001) 297–304.
[71] V. de Serrano, J. D'Antonio, S. Franzen, R.A. Ghiladi, Acta Crystallogr. D Biol. Crystallogr. 66 (2010) 529–538.
[72] B.R. Gelin, M. Karplus, Proc. Natl. Acad. Sci. 74 (1977) 801–805.
[73] J. Baldwin, C. Chothia, J. Mol. Biol. 129 (1979) 175–220.
[74] K. Han, A.S. Woodin, E.D. Lincoln, T.K. Fielman, B. Ely, Mar. Biotechnol. 3 (2001) 287–292.
[75] E. Chiancone, M. Brenowitz, F. Ascoli, C. Bonaventura, J. Bonaventura, Biochim. Biophys. Acta Protein Struct. 623 (1980) 146–162.
[76] J.M. Laine, M. Amat, B.R. Morgan, W.E. Royer, F. Massi, Biochemistry 53 (2014) 7199–7210 (American Chemical Society).
[77] F. Yang, G.N. Phillips Jr, J. Mol. Biol. 256 (1996) 762–774.
[78] J. Zhao, S. Franzen, J. Phys. Chem. B 117 (2013) 8301–8309 (American Chemical Society).
[79] J. D'Antonio, R.A. Ghiladi, Biochemistry 50 (2011) 5999–6011 (American Chemical Society).
[80] S. Jiang, I. Wright, P. Swartz, S. Franzen, Biochim. Biophys. Acta, Proteins Proteomics 1834 (2013) 2020–2029.
[81] X.-j. Song, Y. Yuan, V. Simplaceanu, S.C. Sahu, N.T. Ho, C. Ho, Biochemistry 46 (2007) 6795–6803 (American Chemical Society).
[82] M.P. Pond, A. Majumdar, J.T.J. Lecomte, Biochemistry 51 (2012) 5733–5747.